Bound States in the Continuum Protected by Reduced Symmetry of Three-Dimensional Open Acoustic Resonators

Bin Jia,[1,¶] Lujun Huang,[2,3,*,¶] Artem S. Pilipchuk,[4,¶] Sibo Huang,[1] Chen Shen,[5] Almas F. Sadreev,[4,†] Yong Li,[1,‡] and Andrey E. Miroshnichenko[3,§]

[1] *Institute of Acoustics, Tongji University, Shanghai, 200092, People's Republic of China*

[2] *School of Physics and Electronic Sciences, East China Normal University, Shanghai, 200241, People's Republic of China*

[3] *School of Engineering and Information Technology, University of New South Wales, Canberra, Northcott Drive, Australian Capital Territory, 2600, Australia*

[4] *L. V. Kirensky Institute of Physics, Federal Research Center KSC Siberian Branch, RAN, Krasnoyarsk 660036, Russia*

[5] *Department of Mechanical Engineering, Rowan University, Glassboro, New Jersey, 08028, USA*

(Received 19 January 2023; revised 2 March 2023; accepted 22 March 2023; published 1 May 2023)

Bound states in the continuum (BICs) have been demonstrated as a powerful tool for trapping acoustic fields in an acoustic resonator. It has been widely recognized that symmetry-protected (SP) BICs result from symmetry incompatibility of some eigenmodes of a resonator with propagating modes of waveguides. The most typical example of SP BIC is the odd eigenmode of the resonator with the eigenfrequency embedded into the propagating band of even propagating eigenmodes of the waveguide. In this work, we consider a more sophisticated case of an acoustic cuboid resonator that is opened by the attachment of two cylindrical waveguides. We show that BICs can be sustained in an open acoustic resonator with reduced symmetry. For symmetrical positions of waveguides, the eigenmodes of the cuboid can also be classified as SP BICs and show different stability against the shifts of waveguides from the positions of symmetry of the cuboid. We fabricate a series of coupled waveguide resonators and experimentally verify the existence of these BICs by identifying the vanished linewidth of Fano resonance in transmission spectra. Besides, we also show that evanescent modes of waveguides play a role in the formation of BICs in a nonaxisymmetric waveguide-resonator system by tuning the angle θ between two waveguides. Consequently, the eigenmodes remain SP BICs for $\theta = 0°$ and $\theta = 180°$ but convert into accidental BICs at $\theta \approx 85°$or $\theta \approx 275°$. Such accidental BICs are also experimentally verified. Our results enrich the understanding of SP BICs and accidental BICs, and provide alternative methods of routing acoustic waves and designing acoustic devices requiring fine spectrum features, such as filters and sensors.

DOI: 10.1103/PhysRevApplied.19.054001

I. INTRODUCTION

Bound states in the continuum (BICs) have emerged as a hot research topic in physics because they provide an alternative platform of achieving high-Q resonances [1–3]. The concept of BICs originated from quantum mechanics and then generalized to acoustics as trapped acoustic modes [4–12], which enable sound trapping in an open acoustic resonator [13–20]. The BICs, regardless of their wave physics, can be classified by physical mechanisms. It has been well established that symmetry-protected (SP) BIC results from symmetry incompatibility of the eigenmodes of a closed resonator with propagating modes of the waveguide. Bolsterli *et al*. treated a special quantum mechanical case in which discrete states occur in the continuum in separable potentials [21]. Similarly, in integrable resonators, a symmetry incompatibility decouples the separated eigenmodes from the propagating modes of the waveguides [22,23]. A similar physics is also revealed in acoustic and microwave waveguides with rigid obstacles placed symmetrically [6,7,24]. Another related scenario is the accidental BICs despite the absence of symmetry arguments. These BICs happen when the coupling between the cavity eigenmode and the mode of the continuum accidentally turns to zero for distortion of the eigenmode. They were demonstrated in an open Sinai billiard [25] or in a coupled waveguide-resonator system by proper attachment of waveguides [20].

*ljhuang@mail.sitp.ac.cn; ljhuang@phy.ecnu.edu.cn
†almas@tnp.krasn.ru
‡yongli@tongji.edu.cn
§andrey.miroshnichenko@unsw.edu.au
¶These authors contributed equally to this work.

Acoustic integrable resonators, such as cylindrical or rectangular ones with separable eigenmodes, grant the spectacular case of BICs because of unique propagating waves in attached waveguides. This wave is constant over the cross section of waveguide $\psi(z) = \psi_0 e^{ik_z z}$, and is defined by only wave number $k_z = \omega/v$, where ω is the frequency of wave and v is the velocity of sound in air. Then, as long as the waveguide is attached symmetrically to the nodal line of the resonator's eigenmode, the coupling of the mode with the continuum turns out to be zero. The most obvious examples of SP BICs occur in a system of a rectangular two-dimensional resonator with attached waveguides, which preserve the mirror symmetry C_{2v} [2]. In a previous study, Huang *et al*. reported a general framework for constructing BICs in coupled waveguided-resonator systems [20], where two waveguides are attached at arbitrary positions of the resonator. Remarkably, the authors found that SP BICs, accidental BICs and general Friedrich-Wintgen BICs can be supported in such a two-port system with either mirror symmetry or inverse symmetry. The transition from two-dimensional systems to three-dimensional (3D) open systems considerably enriches the complexity of BICs, which goes far beyond what we have considered in the previous study because two cylindrical waveguides can be placed at arbitrary positions of a cuboid or cylinder resonator. For example, there are SP BICs based on symmetry incompatibility of continua of waveguides with eigenmodes of closed resonator if the axisymmetric cylindrical resonator is attached coaxially with two cylindrical waveguides [10,13]. The case of open systems with broken axial symmetry supports a number of FW BICs [10,13] and seems not to leave room for SP BICs. However, the arbitrary positions of attached waveguides allow for exploring BICs that may not be covered in the previous work.

In the present paper, we consider an open nonaxisymmetric system, as shown in Fig. 1. Two waveguides are attached to a cuboid or cylindrical resonator while one cylindrical waveguide is shifted relative to the center line of resonators. We show that there is a large room for existence of SP BIC owing to reduced symmetry, which is useful for practice because of their robustness. Moreover, as the waveguides smoothly shift relative to the resonator, we reveal a series of accidental BICs at definite positions of waveguide. We show that eigenmodes of a cuboid become the SP BICs for proper attachment of waveguides that preserve mirror symmetry of the total system. We find that these SP BICs have different stability against the perturbation. We experimentally demonstrate these SP BICs by fabricating a series of coupled waveguide-cuboid-resonator systems with 3D printers and measuring their reflection and transmission spectra. The appearance of BICs is verified by the collapse of Fano resonances in the reflection and transmission spectra. We also verify accidental BICs in such a coupled waveguide-resonator system, where one cylindrical waveguide is rotated with respect to the other. Our results may promote the understanding of SP BICs and accidental BICs. They may pave the way for promising applications in enhanced acoustic emission, sensors, filters, etc.

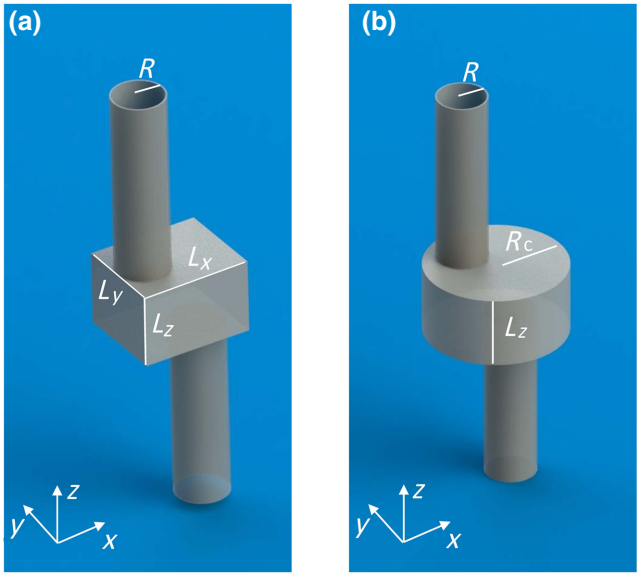

FIG. 1. Schematic illustration of a coupled (a) waveguide-cuboid and (b) cylinder resonator system.

II. RESULTS AND DISCUSSION

A. BICs in coupled waveguide-resonator systems

We consider a coupled waveguide-resonator system as shown in Fig. 1, where two waveguides are attached to two sides of a cuboid or cylinder resonator. Note that two cylindrical waveguides do not share the same axis, and the structural symmetry of the whole system is no longer maintained. We calculate the eigenmodes and eigenfrequencies of resonators, which become complex after attachment of waveguides by use of effective non-Hermitian Hamiltonian complementing commercial software COMSOL Multiphysics based on the finite-element method [14]. The complex eigenfrequencies can be written as $\omega = \omega_0 - i\gamma$, where ω_0 and γ are the resonant frequency and radiative decay rate of leaky modes, respectively. Then, the radiative Q factor can be calculated by ratio $Q = \omega_0/2\gamma$. Thus, searching for BICs in such a system is equivalent to finding eigenmodes with infinite Q factors.

For the sake of simplicity, we choose the radii of two cylindrical waveguides as $R = 14.5$ mm, and the dimensions of cuboid resonators are $L_x = 60$ mm, $L_y = 50$ mm, and $L_z = 50$ mm, respectively. We find a lot of BICs when the projected planes for both waveguides in the x-o-y plane obey the mirror symmetry with respect to the x axis. In particular, we focus on the two simplest examples of SP BICs,

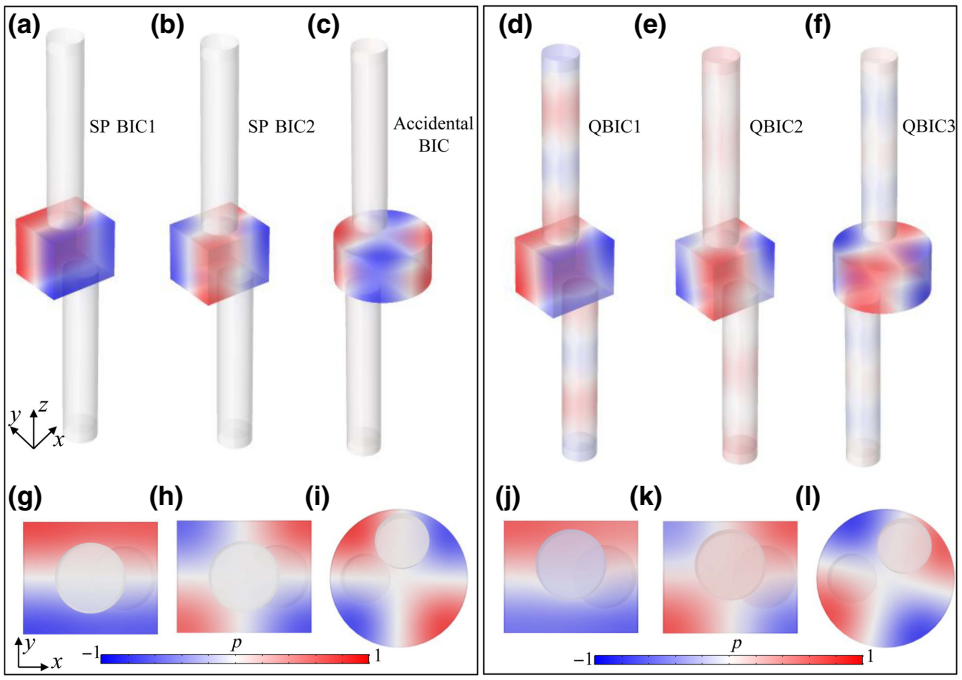

FIG. 2. Schematic illustration of BICs and QBICs. (a)–(c) Eigenfield distributions of two SP BICs and accidental BICs. (d),(e) Eigenfield distributions of the corresponding three QBICs. (g),(i) Eigenfield distributions of three BICs in *x-o-y* plane. (j),(l) Eigenfield distributions of three QBICs in the *x-o-y* plane.

which are modes M_{121} and M_{221} provided that cylindrical waveguides are positioned at mirror symmetry relative to $x/y \to -x/-y$. The eigenfield distributions of two SP BICs are shown in Figs. 2(a) and 2(b). Their eigenfield distributions in the *x-o-y* plane are shown in Figs. 2(g) and 2(h).

To transit from BICs to QBICs, we fix the projected circle center of the bottom waveguide $x_{c2} = 45.5$ mm and $y_{c2} = 0$ mm while the top waveguide has a fixed $x_{c1} = L_x/2 = 30$ mm but varied $y_{c1}(y_{c1} = \delta_y + L_y/2)$, as schematically shown in Fig. 3(a). Figures 2(d) and 2(e) show the eigenfield distributions of two QBICs at $y_{c1} = 5$ mm while Figs. 2(j) and 2(k) display their eigenfield distributions in the *x-o-y* plane. The Q factors of these two QBICs versus y_{c1} are calculated and shown in Fig. 3(b). Indeed, the Q factors of both modes show different trends with the increasing δ_y due to the broken in-plane symmetry. The Q factor of mode M_{221} is several orders higher than that of mode M_{121}. If the center of the top waveguide is moved along the diagonals, the Q factor of mode M_{221} decreases much faster with $\delta_x = \delta_y = \delta_{xy}$ increasing compared to that along the y axis, but their

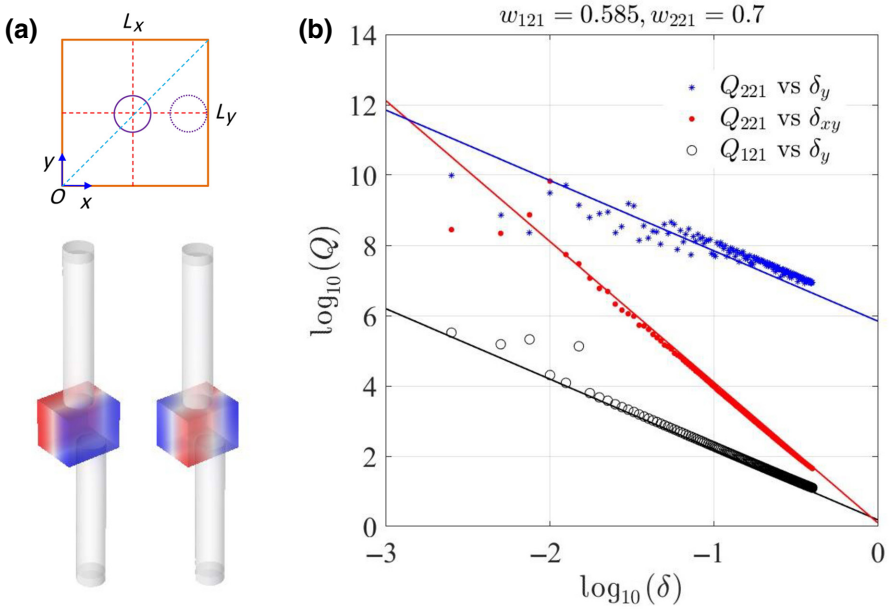

FIG. 3. (a) Top panel is a schematic drawing of the projected image of structure in the *x-o-y* plane. The bottom panel is the eigenfield distribution of BIC modes M_{121} and M_{221}. (b) Q factors of QBIC M_{121} and M_{221} versus δ_y and δ_{xy} when the top waveguide moves along y axis and diagonal.

value is still higher than that of mode M_{121}. Carefully fitting these curves suggests that $Q_{121} \sim A\delta_y^{-2}$, $Q_{221} \sim B\delta_y^{-2}$, $Q_{221} \sim C\delta_{xy}^{-4}$, where A, B, C are the fitted constants. Thus, we conclude that QBIC M_{221} is more stable than QBIC M_{121}, suggesting an effective way of achieving high-Q resonances. A similar phenomenon can be found for QBIC M_{122} and M_{222}, as demonstrated in Fig. S1 within the Supplemental Material [30]. Thus, the nature of SP BIC is preserved as long as in-plane symmetry is preserved (see Fig. S2 within the Supplemental Material [30]). It is noteworthy that such SP BICs also exist in a cylinder resonator shown in Fig. S3 within the Supplemental Material [30].

Next, we consider the case of a cylindrical resonator. The radii of the waveguides and the cylindrical resonator are $R = 14.5$ mm and $Rc = 40$ mm, respectively. The resonator's height is $L_z = 40$ mm. Here, the top waveguide is rotated by θ with respect to the bottom waveguide, as shown in Figs. 1(b) and 4(a). Except for the SP BICs, such a system also supports accidental BICs by choosing the proper rotation angle. One example of accident BICs is shown in Figs. 2(c) and 2(i). The eigenfield distribution of a QBIC is shown in Figs. 2(f) and 2(l). This BIC is classified as an accidental BIC as the whole structure no longer obeys the project-plane symmetry. Also, the position of the attached waveguide is not located at the node of the eigenfield. This type of BIC has been predicted by Lyapina *et al.* [15]. Here, we revisit how such BICs are formed. Without loss of generality, we focus on modes M_{211A} and M_{211B} according to mode definition in cylindrical coordinates. Figure 4(b) shows the eigenfield distribution of four BICs while the top waveguide is rotated by θ. Both the Q factors and resonant frequencies of modes M_{211A} and M_{211B} are calculated and shown in Figs. 4(c) and 4(d). Here, it is worth noting that the mode definition in such a cylinder system differs from that of a cuboid system. The eigenmodes are denoted as M_{mnl}, where m is the azimuthal mode number, n is the radial order number, and l is the order number in the z axis. For M_{211A}, it can be clearly seen that two BICs emerge at $\theta = 0°$ and $\theta = 180°$, which correspond to project-plane SP BICs. For M_{211B}, two BICs are observed at $\theta \approx 85°$ and $\theta \approx 275°$. Obviously, the whole structure does not follow project-plane symmetry. Thus, we classify these types of BICs as accidental BICs. Shown in Fig. 4(d) are the resonant frequencies of two modes as a function of θ. Due to the coupling between the waveguide and the resonator, their eigenfrequencies exhibit oscillation as θ varies. More examples of accidental BICs can be found in Fig. S4 within the Supplemental Material [30].

B. Physical mechanism of BICs

We apply the previously developed effective non-Hermitian Hamiltonian method to explain why the above BICs are formed. To make our conclusion as general as possible, we assume the radius of the cylindrical waveguide as $R = 1$, the other dimensions are measured in terms of R. The resonator length is L_z. The z coordinates of the bottom and top surfaces of the cylindrical resonator are $z = 0$ and $z = L_z$, respectively.

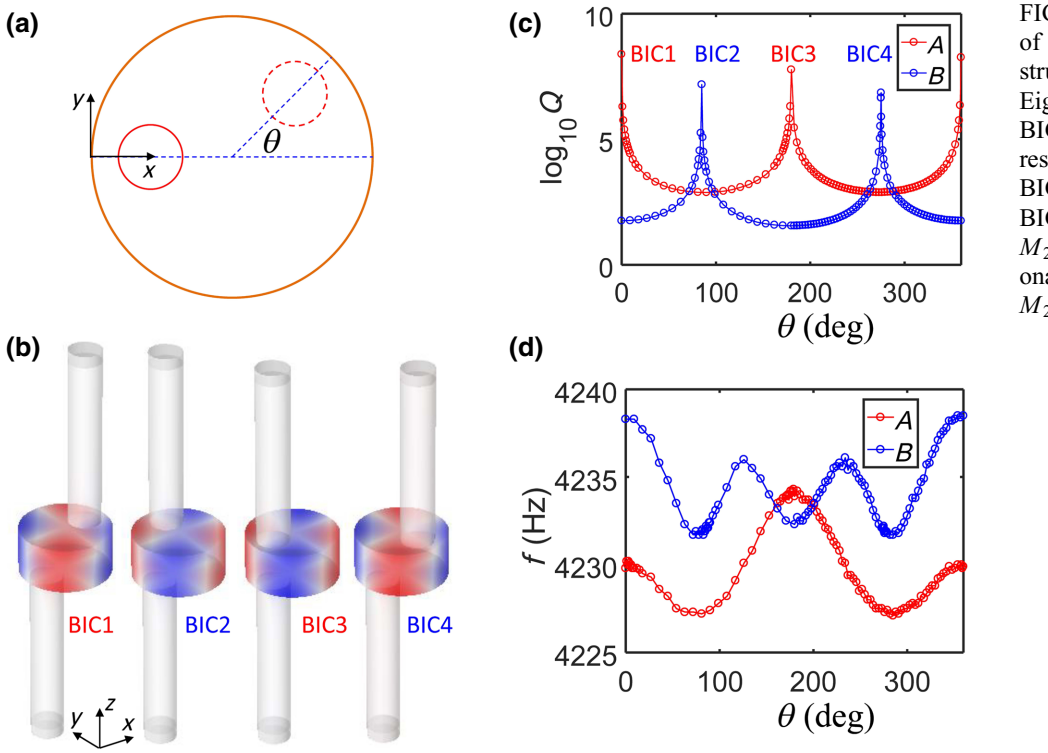

FIG. 4. (a) Schematic drawing of the projected image of the structure in the x-o-y plane. (b) Eigenfield distribution of four BIC modes. BIC1 and BIC3 correspond to SP BICs, BIC2 and BIC4 correspond to accidental BICs. (c) Q factors of M_{211A} and M_{211B} as a function of θ. (d) Resonant frequencies of M_{221A} and M_{211B} as a function of θ.

1. SP BIC in cuboids

To consider SP BICs in the coupled waveguide-resonator system, we present the solutions of the eigenvalue problem in each subsystem. The first two eigenmodes of cuboid according to Eq. (A1) in Appendix A have the following form:

$$\psi_{211} = C_{211}\cos\left(\frac{\pi x}{L_x}\right), \psi_{121} = C_{121}\cos\left(\frac{\pi y}{L_y}\right),$$
$$\psi_{221} = C_{221}\cos\left(\frac{\pi x}{L_x}\right)\cos\left(\frac{\pi y}{L_y}\right). \quad (1)$$

Here all dimensional sizes of the resonator are measured in terms of waveguide radius R. In what follows, we consider only the BICs embedded into the first propagating channel with real k_{01} described by function

$$C_{01}J_0(\mu_{01}r)e^{ik_{01}z} = C_{01}e^{ik_{01}z}. \quad (2)$$

Here $k_{01} = \nu$ is the wave vector, $J_0(x)$ is the zero order of the Bessel function of the first kind, $J_0(\mu_{01}r) = J_0(0) = 1(\mu_{01} = 0)$, $C_{01} = 1/\sqrt{\pi k_{01}}$ is the normalization constant, and normalized frequency is above the first propagation cutoff frequency $\nu > \mu_{01} = 0$ but below the second cutoff frequency $\nu < \mu_{11} = 1.84$.

If the waveguide is positioned at the center of the cuboid side $x_0 = (L_x/2)$, $y_0 = (L_y/2)$, obviously the coupling of the eigenmodes of cuboid with the first continuum equals zero to qualify them as SP BICs. The coupling of the eigenmodes with waveguide shifted from the center by vector $\delta = (\delta_x, \delta_y)$ can be evaluated analytically as presented in Appendix A. In particular, we have

$$W_{121;01} \approx \omega_{121}\delta_y, W_{221;01} \approx \omega_{221}\delta_x\delta_y, \quad (3)$$

where

$$\omega_{121} = J_1\left(\frac{\pi}{L_y}\right)\sqrt{\frac{2L_y}{\pi k_{01}L_xL_z}},$$
$$\omega_{221} = \sqrt{\frac{L_x^2+L_y^2}{L_xL_yL_z}}J_1\left(\frac{\pi}{\sqrt{L_x^2+L_y^2}}\right).$$

We perform analysis of BICs based on the effective Hamiltonian, which in general has the following form [14,15]:

$$\mathbf{H}_{\text{eff}} = \mathbf{H}_B - i\sum_{C=L,R}\sum_{pq}k_{pq}W_{c,pq}W^{+}_{C,pq}, \quad (4)$$

where the matrix $\mathbf{W}_{c,pq}$ is the columns of matrix elements $\mathbf{W}_{mnl,pq}$ for the bottom $z = 0$ and top $z = L_z$ waveguides for each continuum pq. The eigenvalues of the non-Hermitian effective Hamiltonian are complex, whose real parts indicate the position of resonances and imaginary parts correspond to the half-width of resonances. The ratio between real parts and imaginary parts gives the Q factor. If only keeping the first open channel of waveguides $p = 0$, $q = 1$, we have approximately the resonant width of the SP QBIC M_{121} . The Q factor $Q_{121} \approx (\omega_{121}^2/2\gamma_{121}) \sim \delta_y^{-2}$. For the case of the SP QBIC M_{221}, we obtain that $Q_{221} \approx (\omega_{221}^2/2\gamma_{221}) \sim \delta_x^{-2}\delta_y^{-2} \sim \delta_{xy}^{-4}$ $(\delta_x = \delta_y = \delta_{xy})$ for diagonal displacement as shown in Fig. 3. This perfectly explains why the Q factor is linearly proportional to δ_y^{-2} for displacement along y axis and δ_{xy}^{-4} for displacement along diagonal $\delta_x = \delta_y = \delta_{xy}$.

2. Accidental BICs at θ ≈ 85° and θ ≈ 275° in a cylindrical resonator

Note that SP BICs also exist in the cylindrical resonator with the angle between two cylindrical waveguides being $\theta = 0°$ or $\theta = 180°$. It can be easily derived $W^L_{111;0q} = 0$ and $W^R_{111;0q} = 0$ by considering the projected plane's symmetry, suggesting the nature of such a BIC as SP BICs [20] though the whole system's symmetry is no longer preserved for $\theta = \pi$. This is reasonable because the integrals only happen at the projected interface. By applying the same procedure to the cuboid resonator in Fig. 1(a), we can also derive $W^L_{121;0q} = W^R_{121;0q} = 0$ and $W^L_{221;0q} = W^R_{111;0q} = 0$. The only difference is the eigenfunction of closed cuboid resonator taking different forms, which has been studied in detail in Ref. [20].

For $\theta \neq 0°, 180°$, the situation becomes a bit complicated for a cylindrical resonator. Intuitively, one expects that for $\theta = 90°$ the eigenmodes $\psi_{2m,n,l}$ are the SP BICs, which are orthogonal to the continuum $p = 0$ as well as the eigenmodes $\psi_{3m,n,l}$ are SP BICs for $\theta = 60°$. However, these cases are not so trivial. Let us consider the case $\theta = 90°$, which supports, for example, the lowest order of the SP BICs

$$\psi_{211} = C_{211}\,J_2(\mu_{21}r/R)e^{i2\phi}, \quad (5)$$

where C_{211} is the normalization constant given in Appendix B and is not relevant for further consideration.

Figure 5(a) clearly shows that this eigenmode is decoupled from the first propagating mode $p = 0$, $q = 1$ of both waveguides provided the angular position of their center lines are exactly located at the nodal lines of the eigenmode positioned at 0° and 90°. The in-plane eigenfield of BIC at $\theta = 85°$ is shown in Fig. 6, where the top waveguide is positioned at $\theta = 0°$ the bottom waveguide is to be shifted by the angle $\theta = 85°$.

To elucidate the origin of this discrepancy, let us consider the effective Hamiltonian given in Eq. (10) with the account of evanescent mode $p = 1$, $q = 1$. Figure 5(b) illustrates the eigenmode ψ_{211} is coupled with the evanescent mode $p = 1$, $q = 1$. Similarly, the eigenmode ψ_{31l} $(l = 1, 2, 3)$ is coupled with the evanescent mode too.

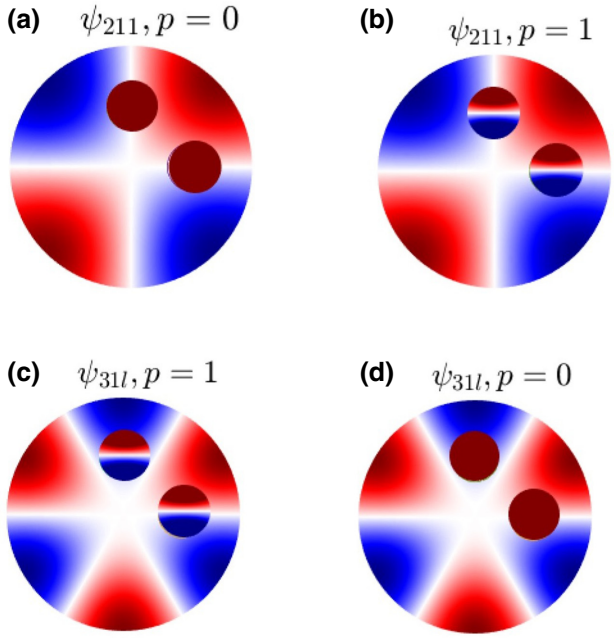

FIG. 5. The pressure fields of eigenmodes with profiles of continua $p = 0,\ 1$ in waveguides attached to the resonator by $\theta = 90°$.

Following the same approach developed in Refs. [2,26], we rewrite the effective Hamiltonian as follows:

$$\mathbf{H}_{\text{eff}} = \tilde{\mathbf{H}}_R - i \sum_{C=L,R} k_{01} W_{C,01} W^{+}_{C,01}, \tag{6}$$

where $\tilde{\mathbf{H}}_R = \mathbf{H}_R + V$, $V \approx |k_{11}| \sum_{C=L,R} k_{01} W_{C,11} W^{+}_{C,11}$ is the Hermitian part of the effective Hamiltonian modified by the evanescent mode $p = 1, q = 1$. As numerics show, the contribution of higher-order evanescent modes is negligible. It is worth noting that the usual two-level approach by accounting for only, for example, eigenmodes ψ_{311} is not sufficient because the coupling constants are $W^{L,R}_{311,01} \approx 0.1$, $l = 1, 2, 3 \ldots$ are equaled by modulus. Moreover, they

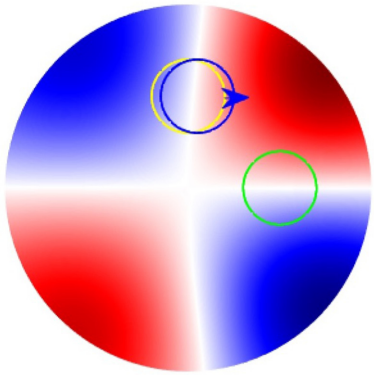

FIG. 6. The pressure field of BICs calculated in full basis given in Eq. (4).

are too small to cause a discrepancy of 5°. Since the contribution of V is small and can be considered by standard perturbation theory that gives

$$\tilde{\psi} = \psi_{211} + \sum_{mnl} \frac{V_{mnl}}{\epsilon_{mnl} - \epsilon_{211}} \psi_{mnl}. \tag{7}$$

Figure 7 shows the coefficients $|a_{mnl}| = |V_{mnl}|/(\epsilon_{mnl} - \epsilon_{211})$. The pressure field of the perturbed mode $\tilde{\psi}$ is shown in Fig. 6.

C. Experimental demonstration of BICs

After gaining a solid understanding of these BICs, we move to demonstrate projected plane SP BICs experimentally. We fabricate a series of coupled waveguide-cuboid-resonators with 3D printing. Figure 8(a) shows the photograph of two typical fabricated samples. The relevant parameters are $d = 29$ mm, $L_x = 60$ mm, $L_y = L_z = 50$ mm. The attached position of the bottom waveguide is fixed with $x_c = 45.5$ mm and $y_c = 0$ mm. The top waveguide is attached at the center of the top surface and is moved along either y axis or diagonal, as schematically shown in Fig. 8(b). According to the simulation results, there are

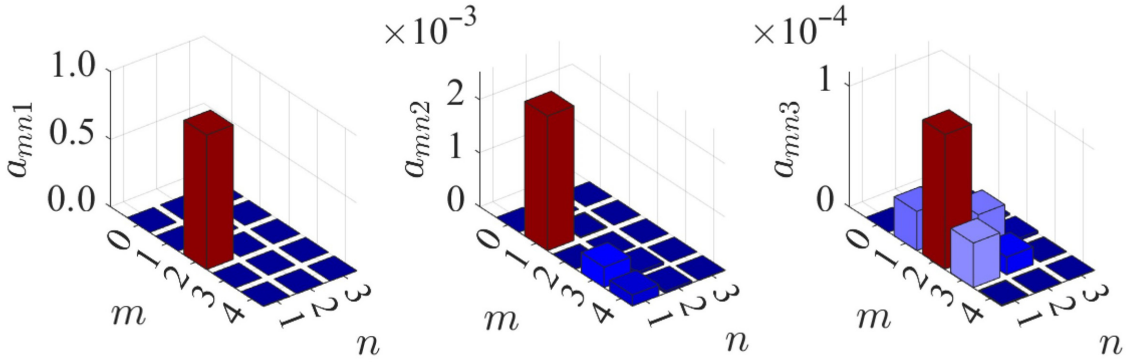

FIG. 7. Coefficients of the perturbation theory expansion.

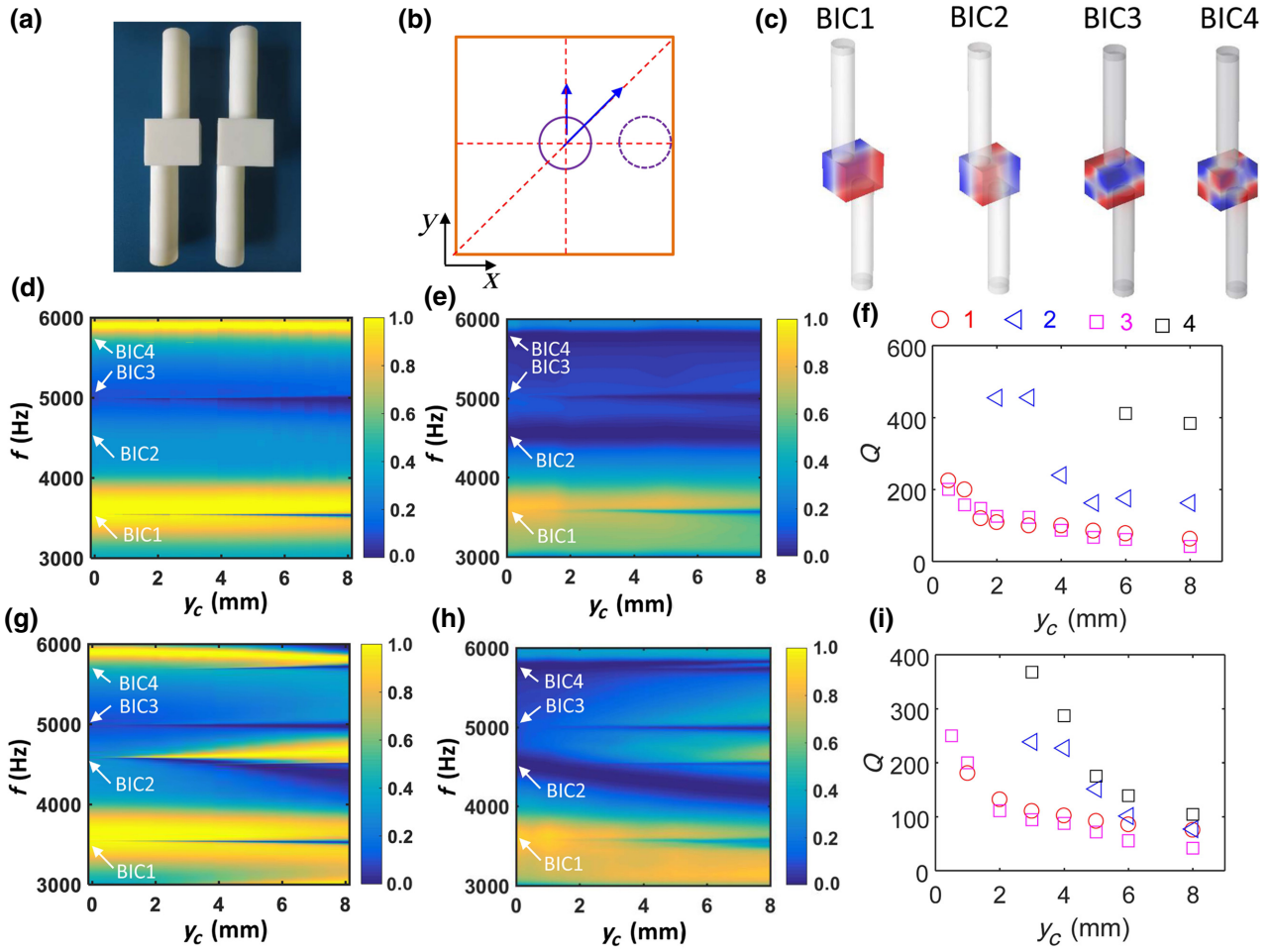

FIG. 8. (a) Photograph of 3D-printed samples. (b) Schematic drawing of projected image in the *xoy*-plane. (c) Eigenfield distribution of four BICs supported by this structure. (d),(e) Simulated and measured transmission spectra mapping for samples with top waveguide moving along the y axis. (f) Retrieved Q factor of four QBICs at different y_c. (g),(h) Simulated and measured transmission spectra mapping for samples with top waveguide moving along diagonal. (f) Retrieved Q factor of four QBICs at different $y_c(x_c = y_c)$.

four BICs below the cutoff frequency of the waveguide, whose eigenfields are shown in Fig. 8(c). The Q factors of these BICs versus y_c have been studied and presented in Fig. 3 and Fig. S1 within the Supplemental Material [30]. We first measure the reflection and transmission spectra of fabricated samples with the top waveguide moving along the y axis. It is clearly seen that four QBICs are shown in the forms of Fano resonance in transmission (or reflection spectra) spectra in Fig. 8(d) [Fig. S5(a) within the Supplemental Material [30]]. The QBIC2 and QBIC4 have narrower resonant linewidth than the other two QBICs. QBIC4 is almost invisible for $y_c < 6$ mm. When y_c is reduced to 0 mm, all four Fano resonances are vanished, indicating the emergence of BICs. To make a comparison, we also calculate the transmission (reflection) spectra mapping in Fig. 8(e) [Fig. S5(b) within the Supplemental Material [30]]. Good agreement can be found between simulation and experiments. Indeed, one can barely see QBIC2 and QBIC4 even at larger y_c due to their larger Q factors. However, QBIC1 and QBIC3 are clearly observed even at $y_c < 2$ mm. We apply the standard Fano fitting procedure to retrieve the measured Q factors of the system [27,28], which are shown in Fig. 8(f). Indeed, QBIC1 and QBIC3 have a relatively smaller Q factor compared to QBIC2 and QBIC4. This is the direct evidence that BIC2 and BIC4 are more stable than BIC1 and BIC3 if the in-plane symmetry is broken along the y axis. This also matches their eigenfield distributions shown in Fig. 8(c), where BIC2 and BIC4 have symmetries with respect to both x and y axes. To further study the stability of different BICs, we introduce symmetry breaking by moving the top waveguide along the diagonal. Figure 8(g) shows the experimentally measured transmission spectra mapping while the reflection spectra mapping is presented in Fig. S5(c) within the Supplemental Material [30]. Indeed, QBIC2 and QBIC4 become visible. However, QBIC2 and QBIC4 still have a larger Q factor than QBIC1 and QBIC3 for the same $y_c(x_c = y_c)$. To make a fair comparison,

numerical simulations on both transmission and reflection spectra mapping are performed and shown in Figs. 8(h) and Fig. S5(d) within the Supplemental Material [30], respectively. One can find an excellent agreement between experiments and simulations. The only difference is that the measured Q factors are lower than the calculated ones due to the thermal viscous losses. However, the Q factors of QBIC2 and QBIC4 are still larger than those of QBIC1 and QBIC3. Thus, these BIC2 and BIC4 may be viewed as ideal candidates for realizing high-Q acoustic resonances.

Next, we move to verify accidental BICs shown in Fig. 4. Figure 9(a) presents the photoimage of fabricated coupled waveguide-cylindrical resonators. Figures 9(b) and 9(c) show the calculated reflection and transmission spectra mapping as functions of angle and frequency. The measured reflection and transmission spectra mapping are plotted in Figs. 9(d) and 9(e). It can be easily found that simulation and experimental results match well. Moreover, one can observe that a Fano resonance appears at around 4290 Hz and its resonant linewidth is reduced to a minimum at 85°, indicating the appearance of BICs. The retrieved Q factor is shown in Fig. 8(f). Good agreement between the experiment and theoretical prediction can be found. The largest Q factor indeed happens at $\theta = 85°$.

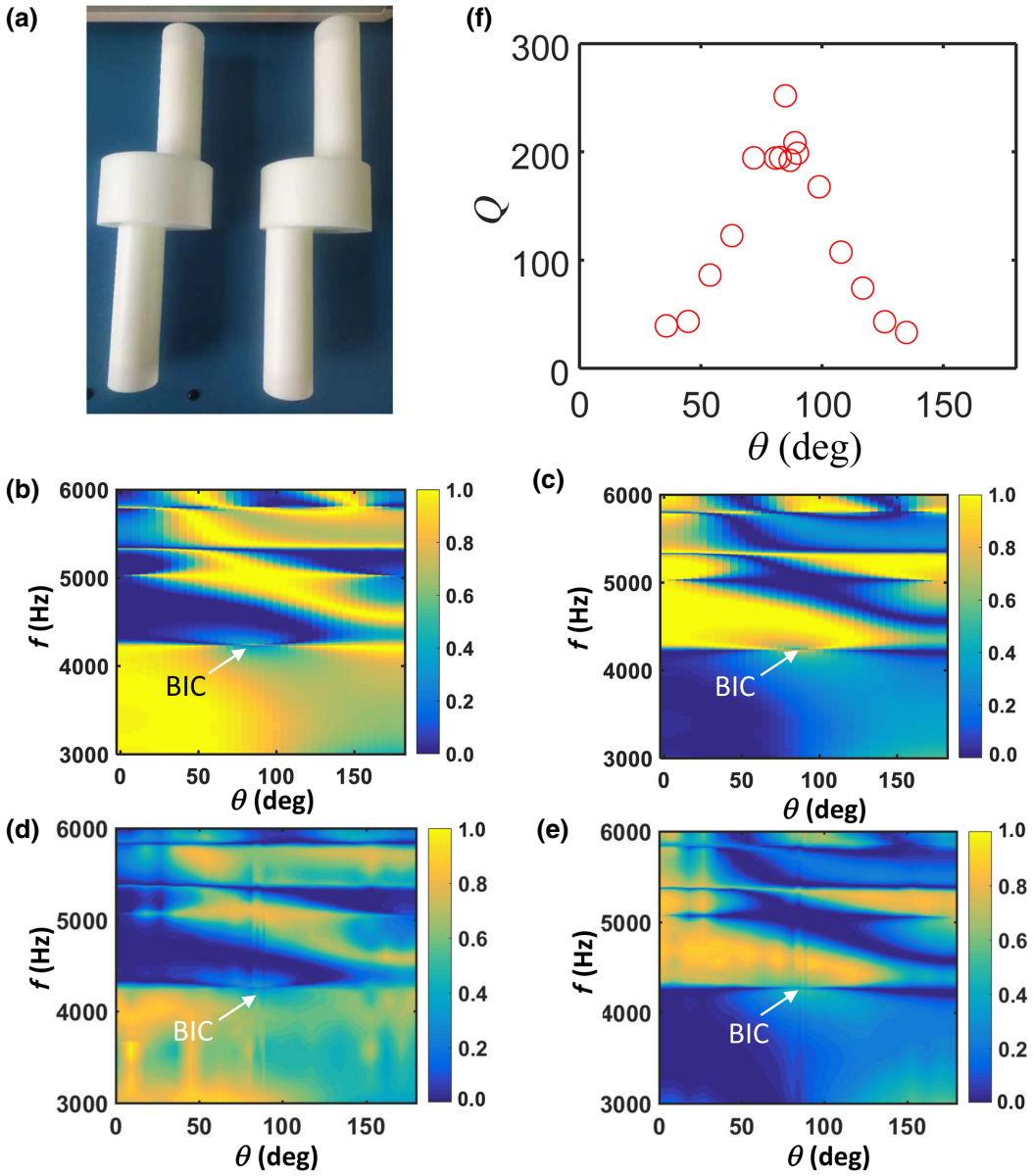

FIG. 9. (a) Photograph of 3D-printed samples. (b),(c) Simulated reflection and transmission spectra mapping versus angle and frequency. (d),(e) Measured reflection and transmission spectra mapping versus angle and frequency. (f) Retrieved Q factor of four QBICs at different angle θ.

Note that the measured Q factor is much lower than the theoretical calculation because of viscosity loss.

III. CONCLUSION

We present a theoretical consideration and experimental demonstration on project plane SP BICs in a coupled waveguide-resonator system. Such a BIC can be transformed into QBICs by breaking the project-plane symmetry. Besides, we find that these BICs show cardinally different dependence on the perturbation, suggesting a viable way of tailoring the Q factor of QBICs. The existence of such BICs is evidenced by the vanishing resonant linewidth in reflection and transmission spectra. In addition, we also confirmed experimentally that such a system supports another type of BICs by tuning the relative angle between two waveguides with respect to the resonators. Our results may generalize the definition of SP BICs and accidental BICs and find promising applications in acoustic sources, sensors, and filters.

IV. MATERIALS AND METHODS

A. Simulations

All simulations in this paper are performed with the commercial software COMSOL Multiphysics. The speed of sound and air density is 343 m/s and 1.29 kg/m^3, respectively. When calculating the eigenmodes and transmission (or reflection spectrum), we apply perfectly matched layer boundaries at the two ends of waveguides to mimic acoustic wave propagation in the infinite space. All other exterior boundaries are set as acoustically rigid.

B. Experiments

The experimental samples are fabricated by 3D-printing technology using laser sintering stereolithography (SLA, 140 μm) with a photosensitive resin (UV curable resin), exhibiting a manufacturing precision of 0.1 mm. The complex transmission (and reflection) coefficients of the samples are measured using a Brüel & Kjær type-4206 T impedance tube with a diameter of 29 mm. A loudspeaker generates a plane wave, and the amplitude and phase of local pressure are measured by four 1/4-inch condenser microphones (Brüel & Kjær type-4187) situated at designated positions. The complex transmission (and reflection) coefficients are obtained by the transfer-matrix method.

ACKNOWLEDGMENTS

L. Huang and A.E. Miroshnichenko were supported by the Australian Research Council Discovery Project (DP200101353) and the UNSW Scientia Fellowship program. B. Jia, S. Huang, and Y. Li are supported by the National Natural Science Foundation of China (Grant No. 12074286), and Shanghai Science and Technology Committee under Grant No. 21JC1405600.

APPENDIX A: CASE OF THE CUBOID RESONATOR

For the closed cuboid resonator ($L_x \times L_y \times L_z$), the eigenfunctions of eigenmodes can be written as

$$\psi_{mnl}(x,y,z) = C_{mnl}\cos\left[\frac{\pi(m-1)x}{L_x}\right]\cos\left[\frac{\pi(n-1)y}{L_y}\right] \times \cos\left[\frac{\pi(l-1)z}{L_z}\right],\ m,n,l = 1,2,3\ldots, \tag{A1}$$

where

$$C_{mnl}^2 = \frac{(2-\delta_{m,1})(2-\delta_{n,1})(2-\delta_{l,1})}{L_xL_yL_z}. \tag{A2}$$

Their corresponding eigenfrequencies are given by

$$\omega_{mnl}^2 = c_0^2\left[\frac{\pi^2(m-1)^2}{L_x^2} + \frac{\pi^2(n-1)^2}{L_y^2} + \frac{\pi^2(l-1)^2}{L_z^2}\right]. \tag{A3}$$

The propagating modes in the hard cylindrical waveguides are specified as

$$\psi_{pq}(r,\phi,z) = \frac{1}{\sqrt{2\pi k_{pq}}}\phi_{pq}(r)\exp(ip\phi + ik_{pq}z), \tag{A4}$$

$$\phi_{pq}(r) = \begin{cases} \frac{\sqrt{2}}{J_0(\mu_{0q})}J_0(\mu_{0q}r), p = 0 \\ \sqrt{\frac{2}{(\mu_{pq}^2-p^2)}}\frac{\mu_{pq}}{J_p(\mu_{pq})}J_p(\mu_{pq}r), p = 1,2,3\ldots \end{cases}, \tag{A5}$$

where p is the azimuthal index ($p = 0,1,2,\ldots$), q is the radial index ($q = 1,2,3\ldots$), r and ϕ are the polar coordinates in the x-o-y plane, and μ_{pq} is the qth root of the equation $((dJ_p(\mu_{pq}r))/dr)|_{r=1} = 0$. The dispersion of each propagating channel is given by

$$\omega^2 = \mu_{mn}^2 + k_{pq}^2. \tag{A6}$$

The coupling matrix element of the eigenmode mnl with the first propagating mode $p = 0, q = 1$ is given by overlapping integral [14,29]

$$W_{mnl;01} = C_{01}\int_0^0 rdr\int_0^{2\pi} d\phi\psi_{mnl}\left(\frac{L_x}{2} + \delta_x + r\cos\phi, \frac{L_y}{2} + \delta_y + r\sin\phi, z = 0\right). \tag{A7}$$

For eigenmode M_{121}, we obtain

$$\begin{aligned} W_{121;01} &= C_{121}C_{01}\int_0^1 rdr\int_0^{2\pi} d\phi \\ &\quad\times\cos\left[\pi\left(\frac{L_y}{2}+\delta_y+r\sin\phi\right)/L_y\right], \\ &= C_{121}C_{01}\sin(\pi\delta_y/L_y)\int_0^1 rdrJ_0(\pi r/L_y), \\ &= 2C_{121}C_{01}L_yJ_1(\pi/L_y)\sin(\pi\delta_y/L_y). \end{aligned} \tag{A8}$$

Similarly, for eigenmode M_{211} we have

$$W_{211;01} = 2C_{211}C_{01}L_xJ_1(\pi/L_x)\sin(\pi\delta_x/L_x). \tag{A9}$$

For eigenmode M_{221}, let us consider a special case shown in Fig. 2(a) when cylindrical waveguide is shifted by vectors $\vec{\delta}=(\delta_x,\delta_y)$, the coupling matrix element of the eigenmode with the continuum $p=0,q=1$ can be expressed as

$$\begin{aligned} W_{221;01} &= C_{221}C_{01}\int_0^1 rdr\int_0^{2\pi} d\phi \\ &\quad\times\cos\left[\pi\left(\frac{L_x}{2}+\delta_x+r\cos\phi\right)/L_y\right] \\ &\quad\times\cos\left[\pi\left(\frac{L_y}{2}+\delta_y+r\sin\phi\right)/L_y\right]. \end{aligned} \tag{A10}$$

An elementary trigonometry gives us

$$\begin{aligned} W_{221;01} &= C_{221}C_{01}\sqrt{L_x^2+L_y^2}J_1\left(\frac{\pi}{\sqrt{L_x^2+L_y^2}}\right) \\ &\quad\times\sin(\pi\delta_x/L_x)\sin(\pi\delta_y/L_y). \end{aligned} \tag{A11}$$

APPENDIX B: CASE OF THE CYLINDRICAL RESONATOR

For the closed cylindrical resonator, assuming its radius is R, its eigenmodes take the following form:

$$\Psi_{mnl}(r,\phi,z)=\sqrt{\frac{1}{2\pi}}\psi_{mn}(r)\exp(im\phi)\varphi_l(z), \tag{B1}$$

where

$$\begin{aligned} &\psi_{mn}(r) \\ &=\begin{cases}\dfrac{\sqrt{2}}{RJ_0(\mu_{0n}R)}J_0\left(\dfrac{\mu_{0n}r}{R}\right), m=0 \\ \sqrt{\dfrac{2}{(\mu_{mn}^2-m^2)}}\dfrac{\mu_{mn}}{RJ_m(\mu_{mn}R)}J_m\left(\dfrac{\mu_{mn}r}{R}\right), m=1,2,3\ldots\end{cases}, \end{aligned} \tag{B2}$$

$$\varphi_l(z)=\sqrt{\frac{2-\delta_{l,1}}{L}}\cos\left[\frac{\pi(l-1)z}{L}\right], l=1,2,3\ldots, \tag{B3}$$

where m is the azimuthal index ($m=0,1,2,\ldots$), n is the radial index ($n=1,2,3\ldots$), l is the axial index ($l=1,2,3,\ldots$), and μ_{mn} is the nth root of the equation $((dJ_m(\mu_{mn}r))/dr)|_{r=R}=0$, which follows from the Neumann boundary condition on the hard walls of hard cylindrical waveguides (air pressure at walls equals zero). The corresponding eigenfrequencies are

$$\omega_{mnl}^2=c_0^2\left[\frac{\mu_{mn}^2}{R^2}+\frac{\pi^2(l-1)^2}{L^2}\right], \tag{B4}$$

where c_0 is the sound velocity.

The coupling matrix elements of these eigenmodes with the first open channel of cylindrical waveguides $p=0,q=1$ given by Eq. (A4) equal [14,15]

$$W_{mnl;01}^C=\int\rho d\rho d\alpha\Psi_{mnl}^*(r,\phi,z=z_C), \tag{B5}$$

where $z_C=0$, L correspond to the bottom and top interfaces of the resonator.

[1] C. W. Hsu, B. Zhen, A. D. Stone, J. D. Joannopoulos, and M. Soljačić, Bound states in the continuum, Nat. Rev. Mater. **1**, 16048 (2016).

[2] A. F. Sadreev, Interference traps waves in an open system: Bound states in the continuum, Rep. Prog. Phys. **84**, 55901 (2021).

[3] L. Huang, L. Xu, M. Woolley, and A. E. Miroshnichenko, Trends in quantum nanophotonics, Adv. Quantum Technol. **3**, 1900126 (2020).

[4] R. Parker, Resonance effects in wake shedding from parallel plates: Some experimental observations, J. Sound Vib. **4**, 62 (1966).

[5] R. Parker, Resonance effects in wake shedding from parallel plates: Calculation of resonant frequencies, J. Sound Vib. **5**, 330 (1967).

[6] M. Callan, C. M. Linton, and D. V. Evans, Trapped modes in two-dimensional waveguides, J. Fluid Mech. **229**, 51 (1991).

[7] D. Evans and R. Porter, Trapped modes embedded in the continuous spectrum, Q. J. Mech. Appl. Math. **51**, 263 (1998).

[8] C. M. Linton, M. McIver, P. McIver, K. Ratcliffe, and J. Zhang, Trapped modes for off-centre structures in guides, Wave Motion **36**, 67 (2002).

[9] Y. Duan, W. Koch, C. M. Linton, and M. McIver, Complex resonances and trapped modes in ducted domains, J. Fluid Mech. **571**, 119 (2007).

[10] S. Hein and W. Koch, Acoustic resonances and trapped modes in pipes and tunnels, J. Fluid Mech. **605**, 401 (2008).

[11] S. Hein, W. Koch, and L. Nannen, Fano resonances in acoustics, J. Fluid Mech. **664**, 238 (2010).

[12] S. Hein, W. Koch, and L. Nannen, Trapped modes and Fano resonances in two-dimensional acoustical duct–cavity systems, J. Fluid Mech. **692**, 257 (2012).
[13] A. A. Lyapina, D. N. Maksimov, A. S. Pilipchuk, and A. F. Sadreev, Bound states in the continuum in open acoustic resonators, J. Fluid Mech. **780**, 370 (2015).
[14] D. N. Maksimov, A. F. Sadreev, A. A. Lyapina, and A. S. Pilipchuk, Coupled mode theory for acoustic resonators, Wave Motion **56**, 52 (2015).
[15] A. A. Lyapina, A. S. Pilipchuk, and A. F. Sadreev, Trapped modes in a non-axisymmetric cylindrical waveguide, J. Sound Vib. **421**, 48 (2018).
[16] S. Huang, T. Liu, Z. Zhou, X. Wang, J. Zhu, and Y. Li, Extreme Sound Confinement From Quasibound States in the Continuum, Phys. Rev. Appl. **14**, 21001 (2020).
[17] L. Huang, Y. K. Chiang, S. Huang, C. Shen, F. Deng, Y. Cheng, B. Jia, Y. Li, D. A. Powell, and A. E. Miroshnichenko, Sound trapping in an open resonator, Nat. Commun. **12**, 4819 (2021).
[18] L. Huang, B. Jia, Y. K. Chiang, S. Huang, C. Shen, F. Deng, T. Yang, D. A. Powell, Y. Li, and A. E. Miroshnichenko, Topological supercavity resonances in the finite system, Adv. Sci. **9**, 2200257 (2022).
[19] A. F. Sadreev, E. N. Bulgakov, A. S. Pilipchuk, A. E. Miroshnichenko, and L. Huang, Degenerate bound states in the continuum in square and triangular open acoustic resonators, Phys. Rev. B **106**, 85404 (2022).
[20] L. Huang, B. Jia, A. S. Pilipchuk, Y. K. Chiang, S. Huang, J. Li, C. Shen, E. N. Bulgakov, F. Deng, D. A. Powell, S. A. Cummer, Y. Li, A. F. Sadreev, and A. E. Miroshnichenko, General Framework of Bound States in the Continuum in an Open Acoustic Resonator, Phys. Rev. Appl. **18**, 54021 (2022).
[21] M. Bolsterli, Continuity of phase shift at continuum bound state, Phys. Rev. **182**, 1095 (1969).
[22] M. Robnik, A simple separable Hamiltonian having bound states in the continuum, J. Phys. A: Math. Gen. **19**, 3845 (1986).
[23] R. L. Schult, D. G. Ravenhall, and H. W. Wyld, Quantum bound states in a classically unbound system of crossed wires, Phys. Rev. B **39**, 5476 (1989).
[24] E. Bulgakov, A. Pilipchuk, and A. Sadreev, Desktop laboratory of bound states in the continuum in metallic waveguide with dielectric cavities, Phys. Rev. B **106**, 75304 (2022).
[25] A. S. Pilipchuk and A. F. Sadreev, Accidental bound states in the continuum in an open Sinai billiard, Phys. Lett. A **381**, 720 (2017).
[26] A. A. Lyapina, A. S. Pilipchuk, and A. F. Sadreev, Bound states with orbital angular momentum in the continuum of cylindrical non-axisymmetric waveguide, Ann. Phys. **396**, 56 (2018).
[27] S. Fan, W. Suh, and J. D. Joannopoulos, Temporal coupled-mode theory for the Fano resonance in optical resonators, J. Opt. Soc. Am. A **20**, 569 (2003).
[28] A. E. Miroshnichenko, S. Flach, and Y. S. Kivshar, Fano resonances in nanoscale structures, Rev. Mod. Phys. **82**, 2257 (2010).
[29] K. Pichugin, H. Schanz, and P. Šeba, Effective coupling for open billiards, Phys. Rev. E **64**, 56227 (2001).
[30] See the Supplemental Material at http://link.aps.org/supplemental/10.1103/PhysRevApplied.19.054001 for Fano resonance fitting, more examples of reduced symmetry-protected BICs and accidental BICs by rotated angle between two waveguides in a three-dimensional open acoustic resonator.